Efficient Charge Generation Via Hole Transfer in Dilute Organic Donor-Fullerene Blends

Yin Song[1], Alexander Schubert[2,3‡], Xiao Liu[4], Srijana Bhandari[3], Stephen R. Forrest[1,4,5], Barry D. Dunietz[3], Eitan Geva[2] and Jennifer P. Ogilvie[1*]

[1]Department of Physics, University of Michigan, Ann Arbor, MI, 48109, USA.
[2]Department of Chemistry, University of Michigan, Ann Arbor, MI, 48109, USA.
[3]Department of Chemistry and Biochemistry, Kent State University, Kent, OH 44242, USA.
[4]Department of Electrical Engineering and Computer Science, University of Michigan, Ann Arbor, MI, 48109, USA.
[5]Department of Material Science and Engineering, University of Michigan, Ann Arbor, MI, 48109, USA.
[‡]present address: Institute of Physical Chemistry, Friedrich Schiller University Jena, 07749 Jena, Germany.
Corresponding Author: * jogilvie@umich.edu

Abstract

Efficient organic photovoltaics (OPVs) require broadband charge photogeneration with near-unity quantum yield. This can only be achieved by exploiting all pathways that generate charge. Electron transfer from organic donors to acceptors has been well-studied and is considered the primary path to charge photogeneration in OPVs. In contrast, much less is known about the hole transfer pathway. Here we study charge photogeneration in an archetypical system comprising tetraphenyldibenzoperiflanthene:C_{70} blends using our recently developed multispectral two-dimensional electronic spectroscopy (M-2DES), supported by time-dependent density functional theory and fully quantum-mechanical Fermi's golden rule rate calculations. Our approach identifies in real time two rapid charge transfer pathways that are confirmed through computational analysis. Surprisingly, we find that both electron and hole transfer occur with comparable rates and efficiencies, facilitated by donor-acceptor electronic interactions. Our results highlight the importance of the hole transfer pathway for optimizing the efficiency of OPV devices employing small-molecule heterojunctions.

Introduction

Organic photovoltaics (OPVs) commonly employ a donor:fullerene acceptor blend heterojunction (HJ) for light harvesting and charge generation. The charge generation process begins with absorption of a photon by either the donor or acceptor, forming an exciton. The exciton migrates to the donor-acceptor junction where the electron transfers to the acceptor or the hole to the donor. Hence, the charge transfer (CT) process is integral to photogeneration. To further improve the device efficiency, therefore, an understanding of the photophysical processes leading to CT is essential(*1-3*). Due to the relatively low extinction coefficients of fullerenes in the solar spectral range, alternative CT pathways initiated by photoexcitation in the acceptor are often neglected. Recently, this concept has been challenged by several reports showing that low donor content devices (<10% weight ratio) can achieve similar or even higher power conversion efficiencies than higher donor content devices,(*3-5*) highlighting the importance of considering the mechanism of charge separation via the hole transfer pathway.

Here we combine multispectral two-dimensional electronic spectroscopy (M-2DES) with time dependent density functional theory (TD-DFT), and rate theory to elucidate the mechanisms of charge transfer at donor-acceptor interfaces. 2DES has emerged as an effective tool to investigate photoexcitation dynamics in complex materials such as photosynthetic systems(*6-9*), organic semiconducting materials(*10, 11*), and quantum dots(*12*). Recently, it has been used to uncover mechanisms of electron transfer in conjugated polymer/fullerene blends,(*10*) although studies on hole transfer are still lacking. TD-DFT electronic structure calculations of dyad models have also been used to simulate complex interfacial processes in OPVs(*13, 14*). In this context, long-range interactions and polarization effects must be accounted for to achieve a reliable description of interfacial CT states(*15*). In this study, we employ an approach based on screened range-separated hybrid functionals (SRSH) recently shown to accurately address condensed phase effects on ground state transport properties(*16*) and excited state properties of solvated pigments.(*17, 18*) The

polarization consistent approach invokes SRSH within a polarized continuum model (PCM) in TDDFT calculations of the excited states. Electronic transition rate constants are then obtained following Fermi's golden rule(*13*) based on the first-principles SRSH-PCM energy parameters. We apply this comprehensive approach to understand charge photogeneration in the archetypal donor-acceptor system comprising dilute tetraphenyldibenzoperiflanthen:fullerene (1:8 DBP:C_{70}) blends.(*4*)

Results

Multispectral two-dimensional electronic spectroscopy

Elucidating the kinetics of hole transfer in DBP:C_{70} blends is complicated by the overlapping absorption spectra of the constituents. The high time and frequency resolution of 2DES is ideally suited for resolving the spectral signatures of different processes that involve separate components of the bulk heterojunction (BHJ) blend.(*19*) More specifically, a 2D frequency spectrum is a map that correlates the photoexcited and the probed states. Compared with conventional pump-probe spectroscopy, the additional excitation axis in 2DES enables direct monitoring of the kinetics of charge generation starting from different initial states. In 2DES, the photoexcited dynamics are encoded in the evolution of three signals: the ground state bleaching (GSB), stimulated emission (SE) and photoinduced absorption (PA). GSB is the nonlinear analog of linear absorption, revealing the loss of ground state molecules due to photoexcitation, or energy or charge transfer. SE is analogous to fluorescence or phosphorescence of the excited molecules, and appears at slightly longer wavelengths than GSB due to vibrational relaxation. PA reveals higher-lying absorptions from excited states including excitons, CT states as well as polarons. A global analysis of the three signals is often required to establish a complete kinetic map of a particular dynamical process. One-color 2DES, which employs the same pump and probe pulses in the visible regime, has been used to investigate electron transfer in OPVs(*10*). However, it is desirable to extend the accessible

frequency range from the visible to the near-infrared (IR) where PA signals of the organic donor and hole polarons are located(*20, 21*).

In this work, we apply multispectral 2DES (M-2DES) using both visible and near-IR probes to investigate charge transfer in the DBP:C_{70} blends. Figure 1b displays absorption spectra of DBP, C_{70} and DBP:C_{70} blends, along with their corresponding pump and probe spectra. The absorption spectrum of DBP exhibits a vibronic progression with the $S_1^{v0} \leftarrow S_0^{v0}$ and $S_1^{v1} \leftarrow S_0^{v0}$ peaks found at wavelengths of λ = 610 nm and 560 nm, respectively. The C_{70} film exhibits a distinct peak at 388 nm and a broad, featureless absorption tail beyond 500 nm with a weak substructure at around 580 nm. These spectra are consistent with SRSH-PCM calculated excited states (see Section S1 and Table S1 in the supporting information (SI) for details). The absorption spectrum of the DBP:C_{70} 1:1 blend film exhibits slightly red-shifted absorption peaks at λ = 613 nm and 563 nm, predominantly owing to the DBP transitions. Interestingly, we find that the absorption spectrum of the blend cannot be fit using a combination of neat DBP and C_{70} absorption spectra (see Figure S1a-c and Section 2 in the SI). This could be caused, on the one hand, by solid state solvation effects due to the different dielectric environments found in the neat films and in the blends(*22*), respectively, and on the other hand, by electronic interactions at the interface that mix the electronic states of the donor and the acceptor. The latter spectral trend is reproduced by calculated electronic excited state energies of the donor-acceptor dyad. Attachment and detachment densities reveal the partly delocalized character of the excited states (see Table S2 of the SI). We find that the absorption spectra of the DBP:C_{70} blends of 1:*n* volume ratios ($n > 1$) are described by a linear combination of the 1:1 DBP:C_{70} blend and the neat C_{70} film, indicating that higher concentrations of C_{70} form clusters in the acceptor-rich blends. This observation is consistent with previous morphological characterizations using X-ray diffraction and transmission electron microscopy(*5*).

Figures 2a and b show the respective absorptive M-2DES spectra of 1:1 and 1:8 DBP:C_{70} blend films at several different delays following excitation. At 0.1 ps the 2D spectra of both blends

exhibit a similar pattern of positive diagonal and cross peaks at ~610 nm and ~570 nm, which are attributed to GSB and SE signals associated with the dominant DBP transitions. A negative signal is observed at 0.1 ps, at detection wavelengths spanning 800-1000 nm, and is assigned to PA of the DBP and C_{70}, consistent with pump-probe (Figure S2) and 2DES (Figure S3) measurements of neat films. These assignments are also consistent with our SRSH-PCM calculations (see Section S1 of SI). In the 1:1 DBP:C_{70} blend, an additional SE corresponding to the $S_1^{v0} \rightarrow S_0^{v1}$ transition appears at λ = 660 nm. This feature is absent in the 1:8 DBP:C_{70} blend, which instead shows a negative PA signal from $\lambda \sim$ 625 nm to 700 nm. This peak is attributed to PA of C_{70}, in accordance with previous studies(*23*) as well as our calculations (Table S1 and Section S1) and pump-probe measurements of C_{70} (Figure S2).

After 3.0 ps, a negative-going feature from 640 nm to 690 nm arises in the 1:1 DBP:C_{70} blend, and lasts for > 1 ns (see Figure S4 in SI). This feature is present at earlier times in the 1:8 DBP:C_{70} blend. It is assigned to PA of the DBP hole polarons based on several observations: 1) The rise of PA from λ = 640 to 690 nm is only seen in blends, suggesting that this species is generated via charge transfer. 2) The GSB of DBP decays much slower than in a neat DBP film, which provides further evidence for the formation of a relatively long-lived CT species. 3) It has been reported that hole-polaron absorption in several conjugated molecules appears at the red edge of the absorption spectrum.(*10, 20, 21*) For example, P3HT films have an absorption peak at 604 nm and a hole polaron absorption band from 640 to 700 nm.(*10, 20, 21*) Absorption of fullerene electron polarons has not been observed in this spectral range,(*23*) and is not expected according to our computational analysis (see Section S1 and Table S1 of the SI). It has been proposed that electroabsorption induced by the adjacent CT state or polarons can also appear on the red side of the donor absorption band. (*24*) However, we exclude this possibility since the transient absorption spectra of blends do not exhibit the characteristic first derivative lineshape associated with electroabsorption, and broadening induced by the electric field of DBP is likely weak owing to its

non-existent dipole moment. In addition, we observe broad spectral band, long-lived PA from 800-1000 nm with a lifetime > 1 ns in both 1:1 and 1:8 DBP:C_{70} blends. We tentatively attribute this feature to absorption by CT states owing to the similar formation and decay rates with PA of the DBP hole polarons.

Global Target Analysis

To quantitatively evaluate the charge generation pathways in the blends, we employ global-target analysis(*25*) of the M-2DES data, finding that three exponential terms are required to obtain a satisfactory fit for both samples. We tested possible models (see Figure S5, Figure S6 and Section S3 in the SI) and find that the model in Figures 3 and 4 provide a consistent picture for both blends. In the case of 1:1 DBP:C_{70} (Figure 3), S1 represents excitons photogenerated inside the DBP domain that migrate to the DBP-C_{70} interface with a time constant of 0.5 ± 0.2 ps. The aggregation of DBP into nanocrystalline domains and their impact on delocalized electronic states at the HJ interface have been investigated previously(*5, 26*). Exciton S2, located near the DBP-C_{70} interface, can be generated either by photoexcitation or energy transfer. It then dissociates into a CT state with a time constant of 3.6 ±0.2 ps. Species-associated spectra of both excitons are composed of GSB and PA of DBP, suggesting that the majority of photons are absorbed by DBP, as expected. We also find that exciton S1 exhibits stronger SE of DBP at ~ 650 nm compared to exciton S2.

To better understand the SE of the two excitons, we measured the temperature-dependent photoluminescence (PL) spectra of the neat DBP film (see Figure S1d in the SI). We find that PL at different temperatures exhibits distinct line shapes. It has a peak intensity at 652 nm at room temperature, and at 690 nm at 77K. These findings support the interpretation of the presence of at least two types of excitons — one with an emission peak that matches the stimulated emission of S1, and the other with an emission peak beyond the probing spectral window of the 2DES measurement. The species associated spectrum for S3 exhibits GSB of DBP and PA of the DBP

hole polaron in the visible and CT state in the near-IR. This finding suggests that both DBP excitons transition into the same CT states.

Figure 4 shows global-target analysis results of the 1:8 DBP:C_{70} blend. In contrast to the 1:1 DBP:C_{70} blend, the S1 component exhibits very different spectral features as well as a longer lifetime (1.0 ± 0.1 ps). The species-associated spectrum for S1 is dominated by PA from λ = 580 nm to 680 nm, which resembles PA of the neat C_{70} film (see Figure S2c in the SI). We, therefore, attribute S1 to the C_{70} exciton, which is expected to be present in considerably higher concentration in the 1:8 DBP:C_{70} blend compared to the 1:1 DBP:C_{70} blend. We find that S2 has a similar spectral profile and lifetime to S2 in the 1:1 DBP:C_{70} blend, which we attribute to DBP excitons generated close to the heterointerface. Compared to the 1:1 blend, the 1:8 DBP:C_{70} blend contain a larger fraction of interfacial and considerably fewer bulk DBP molecules. Thus, the 1:8 DBP:C_{70} blends should exhibit predominantly interfacial rather than bulk DBP excitons, indicating that our interpretation of the S2 exciton is consistent in blends with both a high and low DBP concentrations. Interestingly, we find that both DBP and C_{70} excitons dissociate into common CT states whose spectral signatures appear in S3. Consistent with our analysis of the 1:1 DBP:C_{70} blend, S3 exhibits PA of the DBP hole polaron in the visible and of the CT states in the near-IR, and has a similar lifetime. This finding suggests that there also exists an efficient charge generation pathway initiated by C_{70} photoexcitation, resulting in hole transfer into DBP.

Theoretical Modelling

Previous studies have shown that CT states can be delocalized over both the DBP and C_{70} domains, and subsequently dissociate into charge separated states.(*5*) Here, we focus on the early time dynamics following photoexcitation that involve multiple excited states. As energy and charge transfer processes strongly depend on the excitation energies, we employ the polarization-consistent SRSH-PCM framework, which has been shown to yield accurate excitation energies for both excitonic and CT states of condensed phase molecular systems.(*16, 18*). Our analysis considers

a DBP-C_{70} complex in its optimized geometry, assuming that delocalization effects become relevant only on later timescales. Accounting for the spectral range of the pump laser (Figure 1b), 25 relevant electronic states have been identified as shown in Figure 5a, alongside the identification of the specific configurations. Within the interfacial model of the molecular complex, only a single excitonic DBP state (state 5) is found. We therefore interpret the occurrence of the second exciton in the 1:1 DBP:C_{70} blend, which is absent in the 1:8 DBP:C_{70} blend, as due to delocalized excitons within the DBP domains.(*5, 26*) A simulation of its fast transition (0.5 ± 0.2 ps) into an interfacial DBP-exciton would require a trimolecular model that goes beyond the scope of this analysis.

Given the foregoing discussion, we restrict our analysis to the interfacial excitonic donor state (state 5, red). However, several C_{70}-excitonic states can be seen: four bright states with significant oscillator strengths are found (states 14,17,19, and 22, orange) as well as multiple dark states of low oscillator strength (6-11,18, blue). CT states are found throughout the energy range (1-4,12,13,15,16,20,21,23-25, green). Most notably, electronic densities of the four lowest CT states (1-4) differ from each other only on the anionic C_{70} site and are, therefore, expected to share the same spectroscopic signature as the DBP hole-polaron PA signal. Further information about the states can be found in Table S2 of the SI.

Six hundred transition rate constants between all 25 states were calculated based on Fermi's golden rule (see SI, Section S4 for further details). To this end, molecular reorganization energies were approximated by characteristic single-molecule deformations for the different transition types. A kinetic model was applied to simulate the population dynamics induced by either a donor or an acceptor exciton reaching the interface. The results are shown in Figure 5b, where the populations of states that share the same electronic properties, as indicated by color in Figure 5a, have been grouped for the sake of clarity. The donor exciton (Figure 5b left panel, red curve) shows a transition via electron transfer into the two lowest CT states (cyan curve), whose DBP hole polaron PA signatures are indistinguishable due to the same electronic configuration on the DBP^+ side.

Furthermore, the combined population of both states are described by a single exponential rise with a time constant of 0.8 ps, corresponding to the single CT rate of an experimentally observed 3.6 ± 0.2 ps (S2 to S3 in Figure 3). Considering the limitations of the dyad approach and the assumptions made within the Fermi's golden rule approach (e.g. the harmonic and perturbative approximations), we view a deviation within one order of magnitude to be in reasonable agreement.

A more complex picture is associated with C_{70} excitons. Immediately upon population of the four C_{70}-localized excitonic states (orange curve) - be it through photoexcitation, or via excitons reaching the donor:acceptor interface - several transitions on the femtosecond timescale occur. These are not resolved experimentally due to their ultrashort lifetimes and the presence of coherent artifacts on this timescale. Two decay channels are dominant: 1) exciton transfer towards the energetically favored DBP site (red), and 2) intramolecular relaxation into lower-lying dark excitonic C_{70} states (blue). Both groups of states are transiently populated for approximately 1 ps. This indicates that efficient Förster resonant energy transfer (FRET) from bright C_{70} states (orange curves in Figure 5b, right panel) towards the DBP (red) occurs at the interface, which is suppressed for the dark C_{70} states (blue) due to their vanishing transition dipole moments. The subsequent slower transitions populate the two lowest CT states (state 1 and 2, cyan). More specifically, they correspond to both electron transfer from the DBP-localized excitonic state (state 5) with an effective time constant of 1.8 ps (corresponding to S1 in the experiment: 3.4 ± 0.2 ps), and hole transfer from the C_{70}-localized excitonic states (6 and 7) with a time constant of 0.7 ps (S2 in the Experiment: 1.0 ± 0.2 ps), which is of the same timescale as hole transport within the DBP domain as determined in previous studies.(*27*) Note that the effective electron transfer time appears to be larger than the direct electron transfer time (0.8 ps) from DBP to C_{70} due to the repopulation of the DBP excitonic state from higher-lying excited states. Overall, we find that both pathways, originating in photoexcitation of either the donor or the acceptor, contribute with approximately equal efficiency to the charge generation process.

Discussion

Ultrafast electron transfer in organic donor/acceptor blends has been reported in previous studies,(*1, 10, 28, 29*) with the time scale ranging from hundreds of femtoseconds to tens of picoseconds. In the 1: 1 DBP:C_{70} blend, we find that excitons - either photoexcited within the DBP domain or at the donor-acceptor interface - transition into CT states within 3.4 ± 0.2 ps. This finding is further verified by computational analysis based on SRSH-PCM electronic structure calculations and Fermi's golden rule-based transition rate constants. A similar electron transfer process has also been observed in the 1:8 DBP:C_{70} blend. As both types of DBP excitons can be efficiently converted into common CT states, we conclude that energy loss is limited by charge separation and recombination, but not by inefficient exciton diffusion to the donor/acceptor interface or the initial CT step.

In the 1:8 DBP:C_{70} blend, we find evidence for a hole transfer pathway following the photoexcitation of C_{70}, which is nearly as likely as electron transfer. We note that Kandada and coworkers reported that charge generation originating from the PCBM exciton is via electron transfer following energy transfer from PCBM to P3HT.(*30*) Our calculations show that such exciton transfer from bright excitonic-C_{70} states competes with intramolecular relaxation to low-lying dark excitonic-C_{70} states that cannot undergo further Förster energy transfer. However, our experiments show no evidence of such energy transfer. This may be rooted in its predicted fast timescale (<0.1 ps), which is inaccessible due to pulse-overlap artifacts,(*31*) and its spectral signatures might be masked by the photogenerated DBP excitons.

In summary, systematic analysis of charge transfer in DBP:C_{70} blends provides insight into the charge generation mechanisms in this archetype OPV system. 2DES studies supported by Fermi's golden rule calculations of transition rates based on energies obtained using the SRSH-PCM framework reveal that the hole transfer from the acceptor significantly contributes to the high power conversion efficiency in the low donor content (1:8 DBP:C_{70}) blend. The fast, 1 ps hole transfer rate indicates that no exciton diffusion occurs prior to hole transfer. Previous X-ray diffraction and

transmission electron microscopy measurements(*5*) show that C_{70} crystalline domains have a size of ~5 nm. These findings imply that C_{70} excitons are delocalized over the crystalline domain. Such delocalization can facilitate hole transfer and subsequent charge separation.(*5, 24*) Another interesting finding is that the CT states are formed at similar rates via both the electron transfer and the hole transfer pathways. These CT states then dissociate into free charge carriers or recombine to the ground state. Our results underscore the importance of considering both electron and hole transfer pathways in the design of next generation OPV devices that minimize energy loss.

Materials and Methods

Sample Preparation

All the films are deposited using vacuum thermal evaporation with a base pressure of ~2×10^{-7} Torr, as described previously. Prior to deposition, both C_{70} and DBP were purified once via vacuum thermal gradient sublimation(*5*). Neat DBP, C_{70}, and DBP:C_{70} blend films (with C_{70} volume concentrations of 50 and 90%) were grown on cover slides (quartz). The thickness of DBP, 1:1 DBP:C70 blend, 1:8 DBP:C70 blend and neat C70 film are 54 nm, 54 nm, 80 nm and 100 nm, respectively.

Spectroscopic Measurements

2DES spectra were measured by using a hybrid diffractive-optics and pulse shaper setup as described previously(*19, 32*). Briefly, a regenerative amplifier (Spectra Physics Spitfire Pro) seeded by a Ti:Sapphire oscillator (MaiTai SP from Spectra Physics) is used as the laser source. The 4mJ, 800 nm, 40 fs, 500 Hz output from the amplifier is split and feeds two home-built two-stage non-collinear optical parametric amplifiers (NOPAs) and one degenerate optical parametric amplifier (DOPA). One NOPA is used as pump beam and tuned to excite the absorption band of DBP and C_{70}. The other NOPA and DOPA is used as the probe. The pump beam is sent through a pre-compensating combination of two gratings and two prisms (termed grism) and then into an acousto-

optic pulse shaper (Dazzler, Fastlite) where a compressed pulse pair with a programmable time delay (t_1) is generated. The probe beam from the NOPA is compressed by another grism. The pump NOPA are compressed to 13 fs using the SPEAR method(*17*). The NOPA probe pulse duration is about 13-15 fs, estimated by fitting the coherent artifact from transient grating measurements of neat DBP film as described in previous study(*17*). The DOPA probe pulse is compressed using a pair of chirp mirrors and is estimated to be about 30 fs in duration by fitting of the pump-probe signal of neat DBP film. The pump and probe pulses are directed to a diffractive-optic imaging system to generate the third-order 2DES signal, which is detected by a CCD camera (Princeton Instruments PIXIS 100B). During the experiments, t_1 is scanned using the Dazzler from 0 to 400 fs with time steps of 10 fs. The pump-probe delay (T) is controlled by an optical delay line (DDS220, Thorlabs Inc.) and scanned from -0.2 to 30 ps for 2DES and from -0.2 ps to 1 ns for pump-probe measurements. A six phase-cycling scheme is used as described previously to remove scattering and background signals(*32*). A shutter added in the probe arm removed residual scattering from the pump. In the experiments, the pulse energy of pump and probe pulses were ~8 nJ and 12 nJ, respectively and the beam waists for both pump and probe were ~200 μm. 2D experiments have been performed at magic angle condition and for at least three times to ensure the reproducibility. The data is analyzed using home-written Matlab scripts. The global-target analysis is performed using CapetView3D (Light Conversion). Fluence dependence studies are also performed to avoid the exciton-exciton, exciton-charge, and charge-charge annihilation in the blend films (figure S7).

Computational Theoretical Methods

Interfacial processes are analyzed based on a DBP-C_{70} dyad model. Additional calculations are performed for single molecules and their ions. Condensed phase effects are addressed by the SRSH-PCM framework(*16, 18*). All ground state optimizations and normal mode calculations are carried out employing density functional theory (DFT) at ωB97X-D/6-31G* level(*33, 34*) within the conductor-like polarizable continuum model (PCM)(*35*). Excited state energies and oscillator

strengths are obtained by the SRSH-PCM-based TDDFT framework(*18*) employing PBEh(*36*) and the 6-31G* basis. Importantly the SRSH–PCM framework achieves a polarization-consistent treatment of the molecular electronic structure affected by the condensed environment represented through the dielectric constant.(*16*) The range separation parameter (γ) is tuned following the $J_2(\gamma)$ scheme(*37*), and is found to be 0.180 $bohr^{-1}$ for C_{70} and 0.110 $bohr^{-1}$ for DBP and the dyad, where alpha is set to 0.2 and beta is reset according to the dielectric constant. The electronic coupling between pairs of dyad states are calculated using the fragment-charge difference method (FCD)(*38*), where the DBP acts as donor and the C_{70} as acceptor region. Static and optical dielectric constants of 3.75 and 1.67, respectively, are used throughout the PCM calculations according to previous studies(*39*). All electronic structure calculations are performed using Q-Chem 5(*40*).

Due to a slight overestimation of SRSH-PCM excitation energies, we first identify relevant states within the spectral width of the pump pulse by comparing the neat DBP and C_{70} absorption spectra to the calculated energies. The state assignment is described in more detail in Section S1 and Table S1 of the SI. In a second step, excited states in the dyad system are categorized to be of excitonic character - predominantly localized either on DBP (state 5) or on C_{70} (6-11, 14, 17-19, 22) or of CT character (1-4, 12-14, 16, 20, 21, 23-25). The C_{70}-state assignment allows to limit the number of relevant dyad states in the pump region around the 580 nm substructure to a total of 25, including four bright C_{70} states and one bright DBP state.

Transition rate constants for each pair of dyad states are calculated based on Fermi's golden rule and invoking the harmonic approximation(*13*), which is presented in detail in Section S4 of the SI and which was widely benchmarked in our previous studies[22-25]. The rate expression is based upon the energetic and structural difference between minima of the initial and the target state. Since a full geometry optimization is not feasible for all relevant dyad states due to multiple curve crossings, we characterize each state by its attachment/detachment density as being either of excitonic character localized on DBP or on C_{70}, respectively, or of CT character. Each transition is

then assigned to one of seven fundamental processes corresponding to (A) exciton, (B) electron, or (C) hole transfer, or intramolecular relaxation either between (D) excitonic C_{70} states or among CT states with relaxation (E) on the DBP^+, (F) the C_{70}^-, or (G) on both sites. For each process, characteristic displacement vectors and normal modes and, thus, Huang-Rhys factors and reorganization energies are obtained from (charged and neutral) single molecule calculations. Together with the 25 dyad states' excitation energies and electronic coupling elements, a total of 600 individual transition rate constants are determined and used in a first-order kinetic simulation. Assuming either direct photoexcitation of interfacial states or exciton migration towards the interface via Förster resonant energy transfer in acceptor-rich blends, initial conditions are either set to the DBP excitonic state or to the four bright C_{70} excitonic states according to their relative oscillator strengths.

References

1. T. M. Clarke, J. R. Durrant, Charge Photogeneration in Organic Solar Cells. *Chem Rev* **110**, 6736-6767 (2010).
2. S. Few, J. M. Frost, J. Nelson, Models of charge pair generation in organic solar cells. *Phys Chem Chem Phys* **17**, 2311-2325 (2015).
3. D. M. Stoltzfus, J. E. Donaghey, A. Armin, P. E. Shaw, P. L. Burn, P. Meredith, Charge Generation Pathways in Organic Solar Cells: Assessing the Contribution from the Electron Acceptor. *Chem Rev* **116**, 12920-12955 (2016).
4. X. Xiao, J. D. Zimmerman, B. E. Lassiter, K. J. Bergemann, S. R. Forrest, A hybrid planar-mixed tetraphenyldibenzoperiflanthene/C70 photovoltaic cell. *Applied Physics Letters* **102**, (2013).
5. X. Liu, K. Ding, A. Panda, S. R. Forrest, Charge Transfer States in Dilute Donor–Acceptor Blend Organic Heterojunctions. *ACS Nano* **10**, 7619-7626 (2016).
6. T. Brixner, J. Stenger, H. M. Vaswani, M. Cho, R. E. Blankenship, G. R. Fleming, Two-dimensional spectroscopy of electronic couplings in photosynthesis. *Nature* **434**, 625-628 (2005).
7. G. S. Engel, T. R. Calhoun, E. L. Read, T. K. Ahn, T. Mancal, Y. C. Cheng, R. E. Blankenship, G. R. Fleming, Evidence for wavelike energy transfer through quantum coherence in photosynthetic systems. *Nature* **446**, 782-786 (2007).
8. E. Collini, C. Y. Wong, K. E. Wilk, P. M. Curmi, P. Brumer, G. D. Scholes, Coherently wired light-harvesting in photosynthetic marine algae at ambient temperature. *Nature* **463**, 644-647 (2010).
9. F. D. Fuller, J. Pan, A. Gelzinis, V. Butkus, S. S. Senlik, D. E. Wilcox, C. F. Yocum, L. Valkunas, D. Abramavicius, J. P. Ogilvie, Vibronic coherence in oxygenic photosynthesis. *Nature Chemistry* **6**, 706-711 (2014).

10. Y. Song, S. N. Clafton, R. D. Pensack, T. W. Kee, G. D. Scholes, Vibrational coherence probes the mechanism of ultrafast electron transfer in polymer-fullerene blends. *Nat Commun* **5**, 7 (2014).
11. A. De Sio, F. Troiani, M. Maiuri, J. Rehault, E. Sommer, J. Lim, S. F. Huelga, M. B. Plenio, C. A. Rozzi, G. Cerullo, E. Molinari, C. Lienau, Tracking the coherent generation of polaron pairs in conjugated polymers. *Nat Commun* **7**, (2016).
12. K. W. Stone, D. B. Turner, K. Gundogdu, S. T. Cundiff, K. A. Nelson, Exciton-Exciton Correlations Revealed by Two-Quantum, Two-Dimensional Fourier Transform Optical Spectroscopy. *Accounts Chem Res* **42**, 1452-1461 (2009).
13. M. H. Lee, E. Geva, B. D. Dunietz, Calculation from First-Principles of Golden Rule Rate Constants for Photoinduced Subphthalocyanine/Fullerene Interfacial Charge Transfer and Recombination in Organic Photovoltaic Cells. *The Journal of Physical Chemistry C* **118**, 9780-9789 (2014).
14. D. E. Wilcox, M. H. Lee, M. E. Sykes, A. Niedringhaus, E. Geva, B. D. Dunietz, M. Shtein, J. P. Ogilvie, Ultrafast Charge-Transfer Dynamics at the Boron Subphthalocyanine Chloride/C60 Heterojunction: Comparison between Experiment and Theory. *The Journal of Physical Chemistry Letters* **6**, 569-575 (2015).
15. Z. Zheng, D. A. Egger, J.-L. Brédas, L. Kronik, V. Coropceanu, Effect of Solid-State Polarization on Charge-Transfer Excitations and Transport Levels at Organic Interfaces from a Screened Range-Separated Hybrid Functional. *The Journal of Physical Chemistry Letters* **8**, 3277-3283 (2017).
16. S. Bhandari, M. S. Cheung, E. Geva, L. Kronik, B. D. Dunietz, Fundamental Gaps of Condensed-Phase Organic Semiconductors from Single-Molecule Calculations using Polarization-Consistent Optimally Tuned Screened Range-Separated Hybrid Functionals. *Journal of Chemical Theory and Computation* **14**, 6287-6294 (2018).
17. Y. Song, A. Schubert, E. Maret, R. K. Burdick, B. Dunietz, E. Geva, J. Ogilvie, Vibronic structure of photosynthetic pigments probed by polarized two-dimensional electronic spectroscopy and ab initio calculations. *Chemical Science*, 8143-8153 (2019).
18. S. Bhandari, B. D. Dunietz, Quantitative Accuracy in Calculating Charge Transfer State Energies in Solvated Molecular Complexes Using a Screened Range Separated Hybrid Functional within a Polarized Continuum Model. *Journal of Chemical Theory and Computation* **15**, 4305-4311 (2019).
19. Y. Song, A. Konar, R. Sechrist, V. P. Roy, R. Duan, J. Dziurgot, V. Policht, Y. A. Matutes, K. J. Kubarych, J. P. Ogilvie, Multispectral multidimensional spectrometer spanning the ultraviolet to the mid-infrared. *Review of Scientific Instruments* **90**, 013108 (2019).
20. J. M. Guo, H. Ohkita, H. Benten, S. Ito, Charge Generation and Recombination Dynamics in Poly(3-hexylthiophene)/Fullerene Blend Films with Different Regioregularities and Morphologies. *Journal of the American Chemical Society* **132**, 6154-6164 (2010).
21. R. Osterbacka, C. P. An, X. M. Jiang, Z. V. Vardeny, Two-dimensional electronic excitations in self-assembled conjugated polymer nanocrystals. *Science* **287**, 839-842 (2000).
22. V. Bulović, A. Shoustikov, M. A. Baldo, E. Bose, V. G. Kozlov, M. E. Thompson, S. R. Forrest, Bright, saturated, red-to-yellow organic light-emitting devices based on polarization-induced spectral shifts. *Chemical Physics Letters* **287**, 455-460 (1998).
23. M. Causa, I. Ramirez, J. F. Martinez Hardigree, M. Riede, N. Banerji, Femtosecond Dynamics of Photoexcited C60 Films. *J Phys Chem Lett* **9**, 1885-1892 (2018).
24. S. Gelinas, A. Rao, A. Kumar, S. L. Smith, A. W. Chin, J. Clark, T. S. van der Poll, G. C. Bazan, R. H. Friend, Ultrafast Long-Range Charge Separation in Organic Semiconductor Photovoltaic Diodes. *Science* **343**, 512-516 (2014).

25. I. H. M. van Stokkum, D. S. Larsen, R. van Grondelle, Global and target analysis of time-resolved spectra. *Biochimica et Biophysica Acta (BBA) - Bioenergetics* **1657**, 82-104 (2004).
26. K. Ding, X. Liu, S. R. Forrest, Charge Transfer and Collection in Dilute Organic Donor–Acceptor Heterojunction Blends. *Nano Letters* **18**, 3180-3184 (2018).
27. O. L. Griffith, X. Liu, J. A. Amonoo, P. I. Djurovich, M. E. Thompson, P. F. Green, S. R. Forrest, Charge transport and exciton dissociation in organic solar cells consisting of dipolar donors mixed with C70. *Physical Review B* **92**, 085404 (2015).
28. G. Grancini, M. Maiuri, D. Fazzi, A. Petrozza, H. J. Egelhaaf, D. Brida, G. Cerullo, G. Lanzani, Hot exciton dissociation in polymer solar cells. *Nat Mater* **12**, 29-33 (2013).
29. A. C. Jakowetz, M. L. Bohm, J. Zhang, A. Sadhanala, S. Huettner, A. A. Bakulin, A. Rao, R. H. Friend, What Controls the Rate of Ultrafast Charge Transfer and Charge Separation Efficiency in Organic Photovoltaic Blends. *J Am Chem Soc* **138**, 11672-11679 (2016).
30. A. R. Kandada, G. Grancini, A. Petrozza, S. Perissinotto, D. Fazzi, S. S. Raavi, G. Lanzani, Ultrafast energy transfer in ultrathin organic donor/acceptor blend. *Sci Rep* **3**, 2073 (2013).
31. S. A. Kovalenko, A. L. Dobryakov, J. Ruthmann, N. P. Ernsting, Femtosecond spectroscopy of condensed phases with chirped supercontinuum probing. *Phys Rev A* **59**, 2369-2384 (1999).
32. F. D. Fuller, D. E. Wilcox, J. P. Ogilvie, Pulse shaping based two-dimensional electronic spectroscopy in a background free geometry. *Opt Express* **22**, 1018-1027 (2014).
33. J.-D. Chai, M. Head-Gordon, Long-range corrected hybrid density functionals with damped atom–atom dispersion corrections. *Phys Chem Chem Phys* **10**, 6615-6620 (2008).
34. V. A. Rassolov, J. A. Pople, M. A. Ratner, T. L. Windus, 6-31G* basis set for atoms K through Zn. *J. Chem. Phys.* **109**, 1223-1229 (1998).
35. J. Tomasi, B. Mennucci, R. Cammi, Quantum Mechanical Continuum Solvation Models. *Chem Rev* **105**, 2999-3094 (2005).
36. J. P. Perdew, K. Burke, M. Ernzerhof, Generalized Gradient Approximation Made Simple. *Phys. Rev. Lett.* **77**, 3865-3868 (1996).
37. T. Stein, L. Kronik, R. Baer, Prediction of charge-transfer excitations in coumarin-based dyes using a range-separated functional tuned from first principles. *J. Chem. Phys.* **131**, 244119 (2009).
38. A. A. Voityuk, N. Rösch, Fragment charge difference method for estimating donor–acceptor electronic coupling: Application to DNA π-stacks. *J. Chem. Phys.* **117**, 5607-5616 (2002).
39. S. L. Ren, K. A. Wang, P. Zhou, Y. Wang, A. M. Rao, M. S. Meier, J. P. Selegue, P. C. Eklund, Dielectric function of solid C70 films. *Applied Physics Letters* **61**, 124-126 (1992).
40. Y. Shao, L. Fusti Molnar, Y. Jung, J. Kussmann, C. Ochsenfeld, S. T. Brown, A. T.B. Gilbert, L. V. Slipchenko, S. V. Levchenko, D. P. O'Neill, R. A. D. Jr, R. C. Lochan, T. Wang, G. J.O. Beran, N. A. Besley, J. M. Herbert, C. Y. Lin, T. V. Voorhis, S. H. Chien, A. Sodt, R. P. Steele, V. A. Rassolov, P. E. Maslen, P. P. Korambath, R. D. Adamson, B. Austin, J. Baker, E. F. C. Byrd, H. Dachsel, R. J. Doerksen, A. Dreuw, B. D. Dunietz, A. D. Dutoi, T. R. Furlani, S. R. Gwaltney, A. Heyden, S. Hirata, C.-P. Hsu, G. Kedziora, R. Z. Khalliulin, P. Klunzinger, A. M. Lee, M. S. Lee, W. Liang, I. Lotan, N. Nair, B. Peters, E. I. Proynov, P. A. Pieniazek, Y. M. Rhee, J. Ritchie, E. Rosta, C. D. Sherrill, A. C. Simmonett, J. E. Subotnik, H. L. W. Iii, W. Zhang, A. T. Bell, A. K. Chakraborty, D. M. Chipman, F. J. Keil, A. Warshel, W. J. Hehre, H. F. S. Iii, J. Kong, A. I. Krylov, P. M. W. Gill, M. Head-Gordon, Advances in methods and algorithms in a

modern quantum chemistry program package. *Phys Chem Chem Phys* **8**, 3172-3191 (2006).

Acknowledgments

General: Y. S. thanks Mikas Vengris for assistance with the CarpetView software. Y.S. thanks Ryan D. Pensack for insightful discussion and comments on the manuscript.

Funding: Y.S., S.F. and J.P.O. acknowledge the support of the National Science Foundation through instrumentation grant #CHE-1428479 and grant #DMR-1905401. Y.S. acknowledges the support of the Natural Sciences and Engineering Council of Canada (NSERC) for a Postdoctoral Fellowship. A.S. is grateful for support by an Institute for Complex Adaptive Matter (ICAM) fellowship, awarded by Kent State University and University of Michigan ICAM branches. B.D.D. is grateful for support by NSF Grant CHE-1362504. E.G. is grateful for support by NSF via Grants CHE-1464477 and CHE-1800325. B.D.D. and E.G. are grateful for support by DOE Grant DE-SC0016501. S.F. acknowledges the support of the U.S. Department of Energy, Office of Science, Basic Energy Sciences, under Award #DE-SC0017971. J.P.O., E.G., and S.F. gratefully acknowledge funding through the Mcubed Program by the University of Michigan.

Author contributions: Y. S., X. L, S. R. F. and J. P. O. conceived and designed the experiments. Y. S. performed ultrafast spectroscopic measurements and data analysis. X. L. prepared the samples and collected absorption and temperature-dependent photoluminescence spectra. A. S., S. B., B. D. D. and E. G. designed and performed simulations and considered their correspondence to the experimental data. The manuscript was written through contributions of all authors.

Competing interests: The authors declare no competing financial interests.

Data and materials availability: The datasets generated during and/or analyzed during the current study are available from the corresponding author on reasonable request.

Figures and Tables

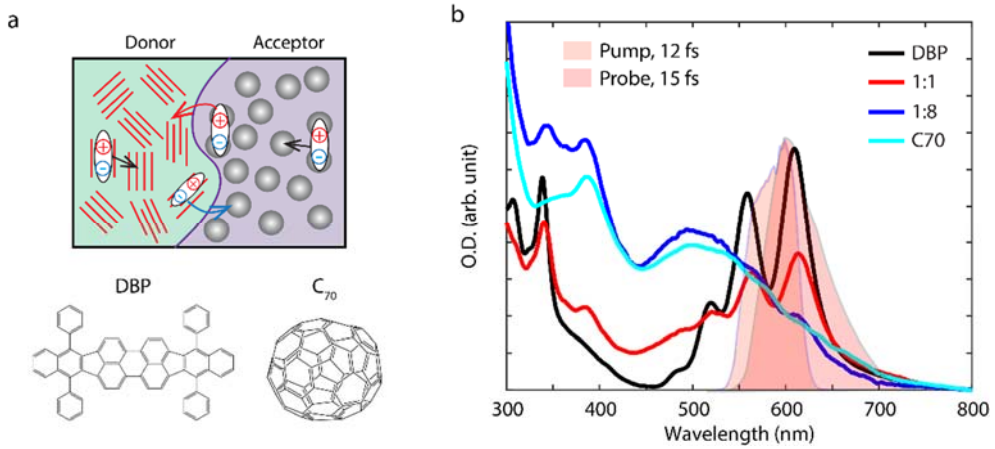

Figure 1 Schematics of charge generation in the DBP:C_{70} blend and the absorption spectra of all samples. a) Two possible charge generation pathways and molecular structures of DBP and C_{70}. b) Absorption spectra of neat DBP film, 1:1 DBP:C_{70} blend, 1:8 DBP:C_{70} blend and neat C_{70} film, along with pump and probe spectra in the visible range.

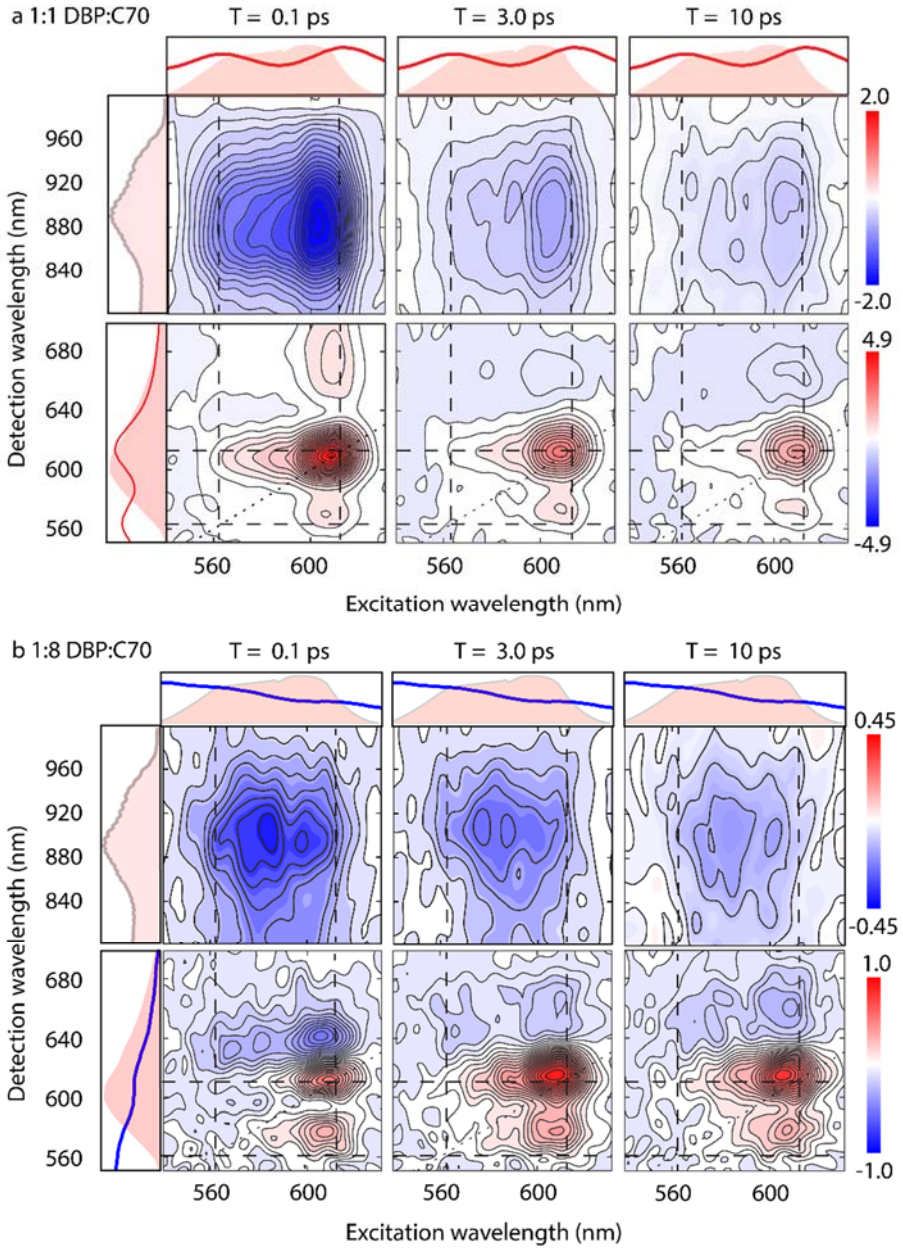

Figure 2 Absorptive 2DES of the DBP:C_{70} blends, alongside with the absorption, pump and probe spectra. a) 2DES of 1:1 DBP:C_{70} blend. Contour interval: 5% of the maximum amplitude. b) 2DES of 1:8 DBP:C_{70} blend. Contour interval: 5% of the maximum amplitude in the visible 2DES and 10% of the maximum amplitude in near-IR 2DES. Dashed lines: 0-0 and 0-1 transitions of the DBP excitonic peaks. Blue solid lines to the left and on top of 2DES: absorption spectra of the DBP:C_{70} blends. Shaded pink: pump and probe spectra.

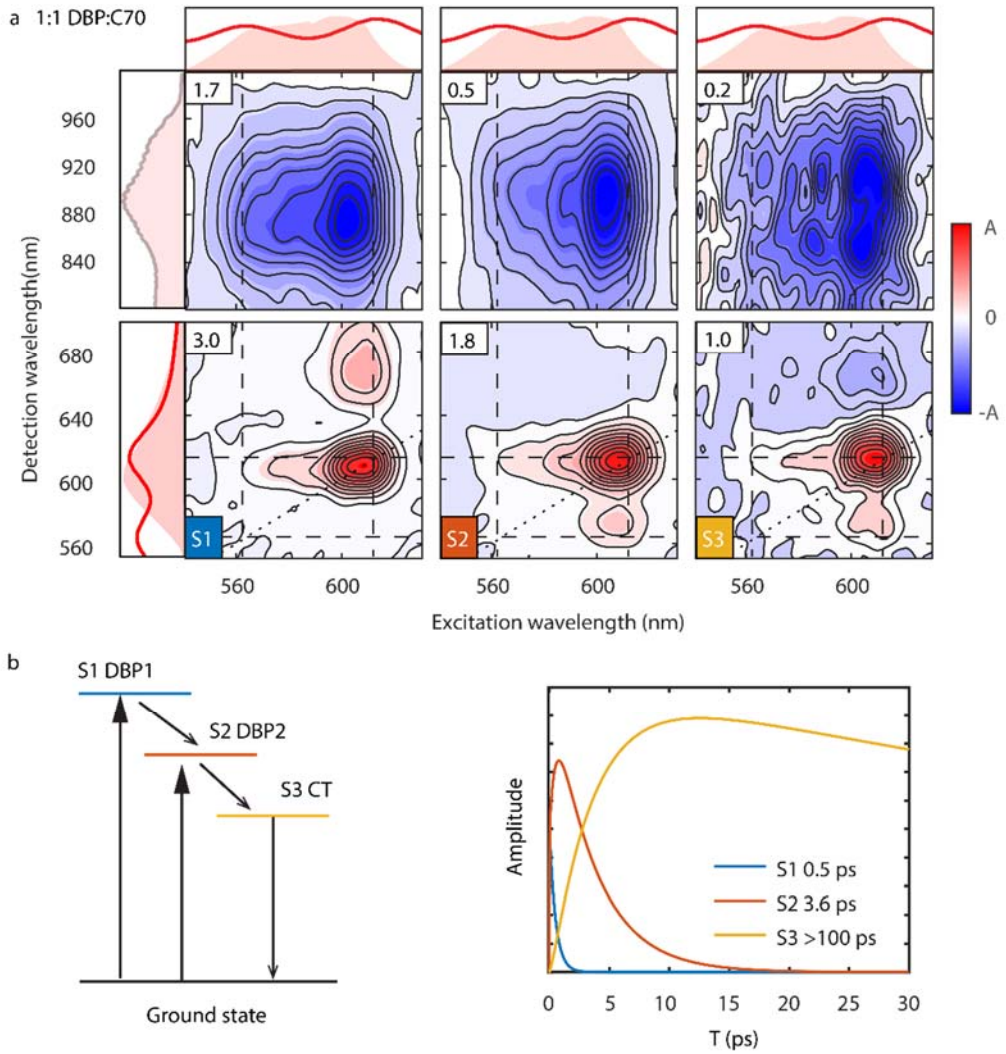

Figure 3 Global-target analysis of the 1:1 DBP:C_{70} blend. a) Species associated spectra of two DBP excitons (S1 and S2) and CT product (S3). Contour interval: 10% of the maximum amplitude (A), which is displayed in the top-left corner of each plot. Dashed lines: 0-0 and 0-1 transitions of the DBP excitonic peaks. Red solid lines to the left and on top of 2DES: absorption spectra of the blend. Shaded pink: pump and probe spectra. b) Kinetic model with two electron transfer pathway used in the analysis and the fitted time traces for two excitons and the CT product.

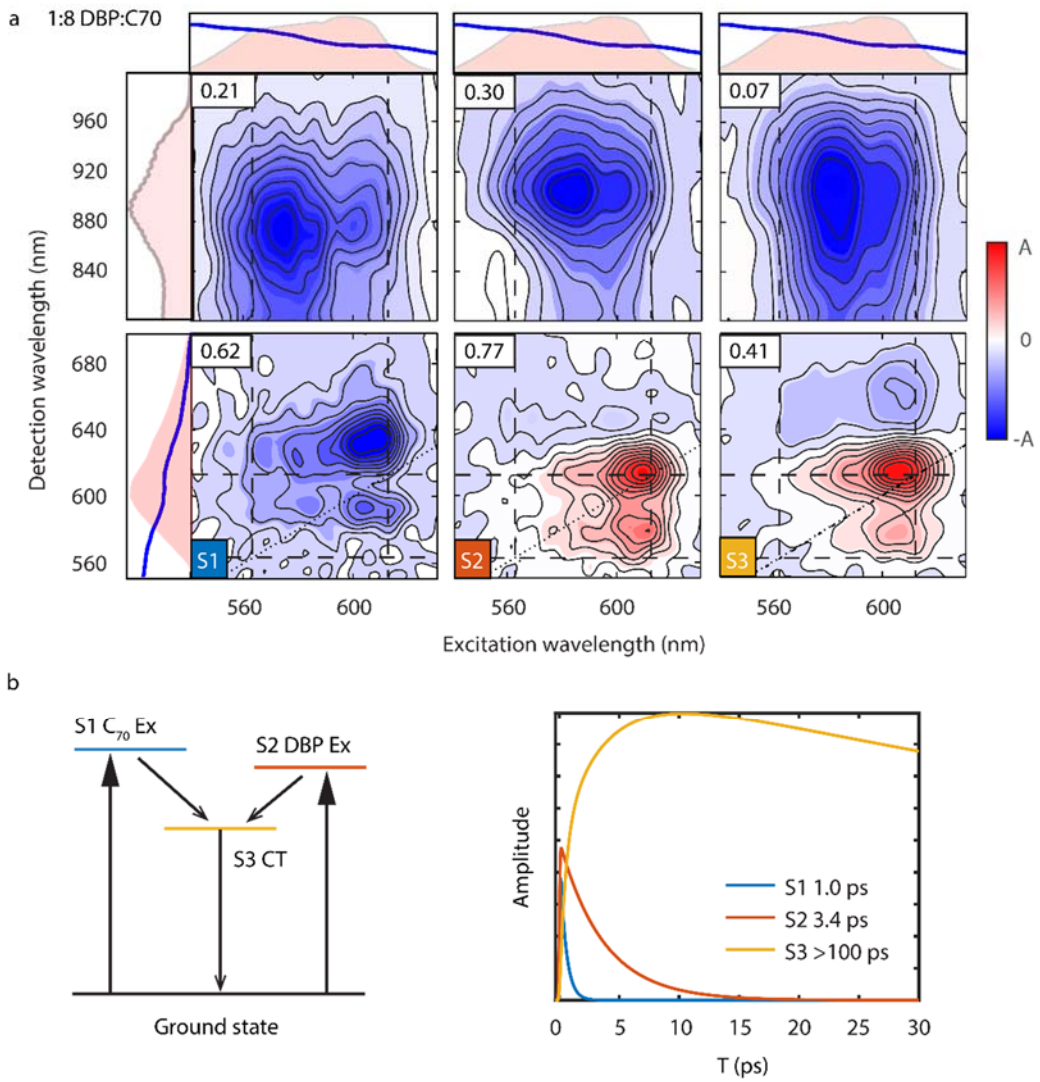

Figure 4 Global-target analysis of the 1:8 DBP:C_{70} blend. a) Species associated spectra of the C_{70} exciton (S1), DBP exciton (S2) and CT product (S3). Contour interval: 10% of the maximum amplitude (A), which is displayed in the top-left corner of each plot. Dashed lines: 0-0 and 0-1 transitions of the DBP excitonic peaks. Blue solid lines to the left and on top of 2DES: absorption spectra of the blend. b) Kinetic model with an electron transfer and a hole transfer pathway and the fitted time traces for S1, S2 and S3.

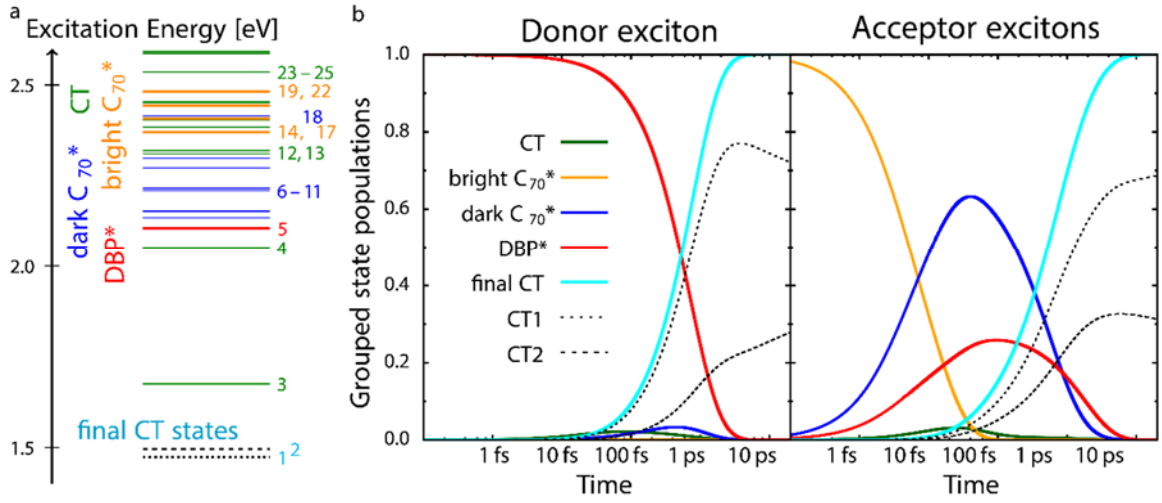

Figure 5 Interfacial excited electronic states of a dyad model and the simulated kinetics.

a) An energy-level diagram of 25 interfacial excited electronic states participating in the photoexcitation and the subsequent formation of two weakly coupled CT states. b) Electron, hole, and exciton transfer kinetics based on the calculated Fermi's golden rule transition rates. Dotted and dashed black lines: simulated population dynamics revealing the formation of two lowest CT states on similar timescales. Cyan curve: combined population dynamics of two lowest CT states, which can be fit exponentially with time constants of 0.79 ps for donor excitons and of 0.84 ps for acceptor excitons.

Supplementary Materials

Supplementary material for this article is in a separated document, which is available at http://